ORIGINAL RESEARCH

Integrating Network Pharmacology and Experimental Validation to Decipher the Mechanism of Action of *Astragalus–Atractylodes* Herb Pair in Treating Hepatocellular Carcinoma

Yuling Liang [1],*, Yuqing Xie [1],*, Xiaoli Liu[1], Lihua Yu [1], Huiwen Yan [1], Zimeng Shang[1], Yuan Wu [1], Xue Cai[2], Wanxin Shi [2], Juan Du[3], Zhiyun Yang [1]

[1]Center of Integrative Medicine, Beijing Ditan Hospital, Capital Medical University, Beijing, 100015, People's Republic of China; [2]Beijing University of Chinese Medicine, Beijing, 100029, People's Republic of China; [3]Beijing Key Laboratory of Emerging Infectious Diseases, Institute of Infectious Diseases, Beijing Ditan Hospital, Capital Medical University, Beijing, 100015, People's Republic of China

*These authors contributed equally to this work

Correspondence: Juan Du, Beijing Key Laboratory of Emerging Infectious Diseases, Institute of Infectious Diseases, Beijing Ditan Hospital, Capital Medical University, Beijing, 100015, People's Republic of China, Email duj656@163.com; Zhiyun Yang, Center of Integrative Medicine, Beijing Ditan Hospital, Capital Medical University, Beijing, 100015, People's Republic of China, Tel +86-10-84322148, Email yangzhiyun2016@163.com

Purpose: Traditional Chinese medicine (TCM) therapy is an important means to treat hepatocellular carcinoma (HCC), *Astragalus* (Latin name: *Hedysarum Multijugum Maxim*; Chinese name: Huangqi, HQ) and *Atractylodes* (Latin name: *Atractylodes Macrocephala Koidz*; Chinese name: Baizhu, BZ) (HQBZ), a classic herb pair, is often used in combination to HCC. However, the main components and potential mechanisms of HQBZ therapy in HCC remain unclear. This study aimed to identify the potential active ingredients and molecular mechanisms of action of HQBZ in HCC treatment.

Methods: The HQBZ-Compound-Target-HCC network and HQBZ-HCC transcriptional regulatory network were constructed to screen the core active compound components and targets of HQBZ therapy for HCC. Molecular docking techniques are used to verify the stability of binding core active compound components to targets. GO and KEGG enrichment analysis were used to explore the signaling pathway of HQBZ in HCC treatment, the mechanism of HQBZ treatment of HCC was verified based on in vivo H22 tumor bearing mice and in vitro cell experiments.

Results: Network pharmacology and molecular docking studies showed that HQBZ treatment of HCC was related to the targeted regulation of IL-6 and STAT3 by the active compound biatractylolide, KEGG pathway enrichment analysis suggest that HQBZ may play a role in the treatment of HCC through IL-6/STAT3 signaling pathway. In vitro experiment results proved that HQBZ could regulate IL-6/STAT3 signaling pathway transduction on CD8+T cells, inhibit CD8+T cell exhaustion and restore the function of exhausted CD8+T cells. In vivo experiment results proved that HQBZ can regulate IL-6/STAT3 signaling pathway transduction in H22 liver cancer model mouse tumor tissue, increased the proportion of tumor infiltrating CD8+T cells.

Conclusion: This study found that HQBZ may play a therapeutic role in HCC by targeting IL-6 and STAT3 through biatractylolide, its mechanism of action is related to regulating IL-6/STAT3 signaling pathway, reversing T cell failure and increasing tumor infiltration CD8+T cells.

Keywords: *Astragalus–Atractylodes* herb pair, hepatocellular carcinoma, IL-6/STAT3 signaling pathway, molecular docking, network pharmacology

Introduction

Primary liver cancer is the third leading cause of cancer death in the world, with an extremely high incidence and mortality rate, of which approximately 75–85% are HCC.[1] T cell exhaustion is an important feature of HCC immune

microenvironment, and many factors such as immunosuppressive cells and cytokines in HCC immune microenvironment, as well as metabolism, can lead to T cell exhaustion. Exhausted CD8^{+}T cells are characterized by high expression of multiple inhibitory receptors, including PD-1, TIM-3, LAG-3, and TIGIT. In addition, exhausted CD8^{+}T cells have impaired ability to produce effector cytokines such as IL-2, IFN-γ and TNF-α, and impaired production of highly expressed inhibitory receptors and effector cytokines promote tumor immune escape.[2] Therefore, reversing T cell depletion and improving tumor immunosuppressive microenvironment are important goals of tumor immunotherapy.

TCM is a major cancer treatment option and studies have shown that Chinese medicine can improve the tumor immunosuppressive microenvironment and restore the immune function of tumor-infiltrating lymphocytes.[3–5] Compatible herb use, a major feature of TCM, can reduce toxicity, increase effectiveness, and expand the scope of drug treatments. Astragalus–Atractylodes herb pair (HQBZ) is a classic clinical herb pair.

Network pharmacology is an emerging discipline that uses network big data to analyze diseases and drug mechanisms. It breaks the traditional thinking of "single disease-single target-single drug" in drug research and development and has an important effect on the creation of new medications, discovery of TCM active compounds, interpretation of drug action mechanisms, analysis of drug combinations, and prescription compatibility laws.[6] This study aimed to identify the potential active compound composition and mechanism of action of the HQBZ herb pair in HCC through network pharmacology, molecular docking, and experimental validation.

Materials and Methods

Identification of HCC Prediction Targets

Obtained from the GEO (https://www.ncbi.nlm.nih.gov/geo/) database GSE62232 microarray dataset,[7] using the database GEO2R online analysis tools to analyze the data after the data set was downloaded, for a corresponding multiple gene probe symbol, keep only the first gene symbol, then delete the duplicate gene symbol and replace it with P<0.05, the obtained targets for the following research.

Target Acquisition for FDA-Approved Liver Cancer Targeting and Immunotherapy Drugs

To supplement the liver cancer-related targets, the DrugBank (https://go.drugbank.com/) database was used to collect the targets of 17 FDA-approved targeted therapy and immunotherapy drugs for HCC,[8] which were merged with those from the GEO database. Duplicate targets were deleted.

Screening of Active Components and Targets of HQBZ

The following databases were utilized to acquire HQBZ components and targets: TCMSP (https://old.tcmsp-e.com/tcmsp.php),[9] UniProt (https://www.uniprot.org/),[10] PubChem (https://pubchem.ncbi.nlm.nih.gov/),[11] and SwissTargetPrediction (http://www.swisstargetprediction.ch/).[12] Drug similarity (DL) refers to compounds found in TCM that are similar to known drugs. Compounds with DL≥0.18 can be identified as drug analogs and have the potential to become drugs. DL-based compound screening can save resources for drug development.[13] The active compounds of HQBZ were retrieved from the TCMSP database and screened according to DL ≥0.18. Simultaneously, the Related Targets function of TCMSP was used to retrieve the related targets of the compound components. The UniProt database was used to convert targets to gene symbols for standardizing the target names. The structures of the active compounds of HQBZ were obtained from the PubChem database, and SwissTargetPrediction was used to gather the pertinent targets of the active compounds according to the screening criteria Probability>0. Finally, the targets from the two processes were combined.

HQBZ–Compound–Target–HCC Network Diagram Construction

The Venny database (https://www.bioinformatics.com.cn/static/others/jvenn/example.html) was used to collect the intersection targets of HQBZ, HCC and the targets from the DrugBank database. Cytoscape visualizes the network and calculate parameters such as degree, betweenness centrality (BC), closeness centrality (CC), and average shortest path length (ASPL) for each node in the network.[14] The degree of a node indicates the number of nodes directly related to it, and the biological

significance of a node increases with its degree. The BC is defined as the percentage of shortest paths across a specific network node and nodes are significant in networks with high BC. The CC is defined as the reciprocal of the sum of the shortest paths from one node to other nodes, and a node is significant in networks with high CC. In addition, the value of a node in the network increases with ASPL. These parameters allow an in-depth analysis of the attributes of the nodes in the interactive network. To investigate the possible active components of HQBZ for HCC, all data were imported into Cytoscape 3.7.2 to construct the HQBZ–Compound–Target–HCC network.

Protein–Protein Interaction Network(PPI) Construction

The intersection targets obtained from the Venny database were imported into the STRING (https://string-db.org/) database to further analyze the protein interaction networks.[15] The selection criteria for organisms were set to "Homo sapiens" according to combined score>0.9 screen. PPI information was entered into Cytoscape 3.7.2 to build a PPI network. Topology analysis, MCODE cluster analysis, ClusterONE cluster analysis on the PPI network using plug-ins included in Cytoscape, and the top 5% target of the four parameters degree, BC, CC, ASPL, were selected from the topological analysis results. The MCODE cluster analysis results were obtained from the top 5% of clusters by scoring from high to low. The ClusterONE cluster analysis results were obtained from the top 5% of clusters using the p-value from small to large. Targets of the three parts were merged to remove duplicates.

Genomic Transcriptional Regulatory Network Between HQBZ and HCC

The human genome transcriptional regulatory network data from the TRRUST (https://www.grnpediötrrust/) database,[16] which contains 795 TF genes, 2067 non-TF genes, and 8427 regulatory link pairs, served as a background for building the HQBZ–HCC transcriptional regulatory networks. The HQBZ–HCC transcriptional regulatory network was constructed using the intersection targets of the HQBZ, 795 TF genes, HCC targets, and 2067 non-TF genes.

GO and KEGG Enrichment Analysis

Metascape (https://metascape.org/gp/index.html#/main/step1) was used for the GO and KEGG analyses.[17] GO assays are used to screen biological process (BP), cell components (CC), and molecular function (MF). KEGG enrichment analysis identified important signaling pathways involved in the genes. The data were then uploaded to the Bioinformatics (http://www.bioinformatics.com.cn/) platform for visualization.

Molecular Docking

Drug research frequently uses molecular docking; computer simulations can be used to forecast the binding patterns and affinities of small compound ligands to large protein receptors. Complete high-throughput and virtual screening of target compounds effectively improves the efficiency of new drug design and discovery, and significantly reduces the expense of developing and researching new drugs.[18]

The PDB (https://www.rcsb.org/) database is the source of the crystal structure of the protein ligand.[19] Protein crystal structures with X-RAY DIFFRACTION<2.5A were selected, downloaded, saved as a PDB format file, and then preprocessed using AutoDock Tools,[20] such as eliminating water molecules, incorporating charges, and introducing hydrogen ions. The output was saved as a PDBQT format protein ligand file. The molecular structures of drug ligands were obtained from the TCMSP database. The active compounds of the target drug were retrieved, and the molecular structure was downloaded and saved as a Mol2 format file. Similarly, the drug ligand structure was processed with AutoDock Tools, charge was added, and the drug ligand file was output in the PDBQT format. The protein receptor PDBQT file was imported into AutoDock Tools to define the docking parameters of the target proteins. Finally, molecular docking was performed using AutoDock Vina and PyMOL software was employed to visualize the molecular docking results.[21]

Experimental Verification

Preparation of Drug-Containing Serum

HQBZ was purchased from Beijing Ditan Hospital Pharmacy of Traditional Chinese Medicine. Then, 450 mL water was added to 20 g HQ and 9 g BZ powder, ground, stirred evenly, soaked for 30 min, decocted twice for 30 min each, filtered, and mixed in a beaker. Twelve SPF-grade male Sprague Dawley rats (200 ± 10 g, 7 weeks of age, acquired from SiPeiFu (Beijing) Biotechnology Co., LTD., China, Certificate No. SCXK (Beijing) 2019–0010), were fed appropriately for a week in a typical animal feeding chamber at 22 ± 2 °C, 60% relative humidity, and a 12-h light and dark cycle. The rats were randomly assigned to HQBZ and control group (each group n=6). The rats in the HQBZ and control groups were given 0.8 mL HQBZ solution and normal saline, respectively, once daily for 1 week in the stomach. Two hours after the last administration, 30 mg/kg pentobarbital sodium was injected intraperitoneally to induce anesthesia and blood was collected from the abdominal aorta under sterile conditions. The blood was centrifuged at 3000 rpm for 10 min, the serum was filtered using a 0.22 μm filter and inactivated at 56 °C for 30 min. The serum of the control group was used as the control serum containing solvent and that of the HQBZ group was used as the medication serum containing HQBZ. Serum and complete medium were mixed at 1:9 volume ratio.

Spleen Cell Culture

A total of 3 healthy male BALB/c mice (SPF grade, 10-week-old, 25 ± 2g) were bought from SiPeiFu (Beijing) Biotechnology Co., LTD. The spleen was separated from the abdominal cavity, ground with a tissue grinding rod in an EP tube containing PBS, filtered through a 200-mesh filter, centrifuged at 1200 rpm for 5 min, cleaved with red cell lysate for 10 min, and then treated with RPMI1640 complete medium to terminate the reaction. The cells were centrifuged at 1200 rpm for 5 min and resuspended in PBS for further use.

Fresh mouse spleen cells (1×10^6 cells/well) were cultured for 24 h in CD3-coated 24-well plates using (1) conditioned medium (2 mmol/L L-glutamine, 10% fetal bovine serum (FBS), and 100 U/mL penicillin and streptomycin) only, (2) conditioned medium supplemented with 40 ng/mL recombinant mouse IL-6 (PeproTech, USA), (3) conditioned medium supplemented with medicinal serum containing 10% HQBZ, (4) 10% control serum was added to the conditioned medium, (5) conditioned medium supplemented with 40 ng/mL recombinant mouse IL-6 and medicinal serum containing 10% HQBZ, or (6) conditioned medium supplemented with 40 ng/mL recombinant mouse IL-6 and 10% control serum. The optimal concentration of HQBZ-containing serum was determined using flow cytometry to detect the proportion of apoptotic cells with Annexin V positive on CD8$^+$T cells (Figure S1). After stimulating for 24h, the cells were collected in a flow tube, centrifuged at 1200 rpm for 5 min, and resuspended in an appropriate volume of PBS. This experiment was repeated three times.

Flow Cytometry Analysis

The immunophenotype of the cells were determined by staining with an anti-mouse monoclonal antibody at room temperature for 30 min in dark and then washing thoroughly for further analysis. For detecting the intracellular cytokines, CD3, CD28, and GolgiPlug (eBioscience, USA) were added to the stimulation process, and the collected cells were used to stain the surface markers, fixed and permeabilized for 30 min, incubated with intracellular antibodies in the dark for 30 min, and then washed for flow cytometry analysis. Flow cytometry was performed on a BD FACSVerse flow cytometer powered by the FACSDiva software (BD Biosciences, USA). FlowJo 10.8.1 software (TreeStar, USA) was used for data analysis. The antibodies and color schemes used are listed in Table S1. The experiment was repeated three times.

H22 Tumor-Bearing Mice Establishment

A total of 30 healthy male BALB/c mice (SPF grade, 12-week-old, 25 ± 2g) were bought from SiPeiFu (Beijing) Biotechnology Co., LTD. The 30 mice were randomly divided into 5 groups: control group, model group, HQBZ-H group, HQBZ-M group and HQBZ-L group (each group n=6). H22 cells were purchased from Beijing Dingguo Changsheng Biotechnology Co., Ltd. (Beijing, China) and cultured in medium containing 10% FBS. Three days later, H22 cells were collected, and 2×10^6 H22 cells were injected into the right axilla of mice in model group and HQBZ group. After 24 hours, the HQBZ group was given 0.2 ml HQBZ liquid (HQBZ-H group 6.52 g/ml; HQBZ-M group 3.26 g/ml; HQBZ-L group 1.63 g/ml) by intragastric administration once a day for 2 weeks.

Immunohistochemical Staining

The prepared tumor tissue paraffin sections were dewaxed with xylene and dehydrated using an ethanol gradient. An EDTA antigen repair solution (pH 9.0, Servicebio) was used to repair the tumor tissue. After incubating with 3% H_2O_2 in dark at room temperature for 25 min, the sections were further incubated with 3% BSA in dark at room temperature for 30 min. Then, they were incubated with primary antibodies (including mouse CD8, IL-6, STAT3 and c-MAF antibodies) in a wet box at 4 °C overnight. The next day, they were incubated with the secondary antibody at room temperature for 50 min. The DAB color development solution was used for color development, and the positive color was brownish-yellow. After collecting the images, ImageJ_v1.8.0 (Wayne Rasband National Institutes of Health, USA) was used to analyze the positive staining rate of the collected images.

Multiple Immunofluorescence

The prepared tumor tissue paraffin sections were dewaxed with xylene and dehydrated using an ethanol gradient. An EDTA antigen repair solution (pH 9.0) was used to repair the tumor tissue. After incubating with 3% H_2O_2 in dark at room temperature for 25 min, the sections were further incubated with 3% BSA in dark at room temperature for 30 min. Then, they were incubated with primary antibodies (including mouse CD8, IL-6, STAT3 and c-MAF antibodies) in a wet box at 4 °C overnight. The next day, they were incubated with the secondary antibody at room temperature for 50 min. The sections were further incubated with DAPI dye solution for 10 min at room temperature in dark. After the images were collected, ImageJ_v1.8.0 software was used to analyze the positive staining rate of the collected images.

Statistical Analysis

Experimental data were analyzed using GraphPad Prism 9.5. Normally distributed data were tested using one-way ANOVA, data with a skewed distribution were tested using the Kruskal–Wallis test, and the post hoc test was performed using Tukey's test. $P < 0.05$ was considered the threshold for statistical significance.

Results

Construction and Analysis of HQBZ–HCC Composite Network

A total of 12,284 and 34 HCC-related targets were obtained from the GEO database gene chip dataset GSE62232 and the DrugBank database, respectively. After combining the two databases to eliminate duplicate targets, 12,300 HCC-related targets were identified.

A total of 38 HQ components and 8 BZ components were obtained from TCMSP, UniProt, PubChem, and SwissTargetPrediction databases. Moreover, 45 active compounds were obtained by combining the active compounds of HQ and BZ, which were used to predict 728 HQBZ-related targets.

HQBZ components and HCC targets were combined using the Venny database, and 433 intersection targets were identified (Figure 1A), which were regarded as potential therapeutic targets for HCC treatment using HQBZ. Cytoscape 3.7.2 integrated 433 targets and 45 effective components of HQBZ against HCC to create the HQBZ–Compound–Target–HCC complex network, which allowed us to investigate the vital components and targets of HQBZ important in HCC treatment (Figure 1B). According to the degree of the topological parameters calculated using Cytoscape 3.7.2 software, the top 10 active compounds were selected as the 10 most important potential active compounds for HCC prevention and treatment. Information regarding these 10 compounds is presented in Table 1.

Protein–Protein Interaction Network Construction and Analysis

To investigate the main targets of therapeutic effects of HQBZ in HCC, a PPI network was constructed. The 433 targets of HQBZ against HCC were submitted to STRING12.0 database, which yielded 2165 interacting targets, of which 408 were presumed HQBZ targets. The network was visualized using Cytoscape 3.7.2 software, as which resulted in a PPI network with 2165 nodes and 20,797 edges (Figure 2A). We ran topology analysis, MCODE cluster analysis and ClusterONE cluster analysis on PPI network and crossed these targets with 433 targets of HQBZ to HCC to get 140 intersection targets (Figure 2B). To create the PPI network, 140 targets were added to the STRING database. A PPI network with 1491 edges and 133 nodes was built using Cytoscape 3.7.2 (Figure 2C), and topological analysis was
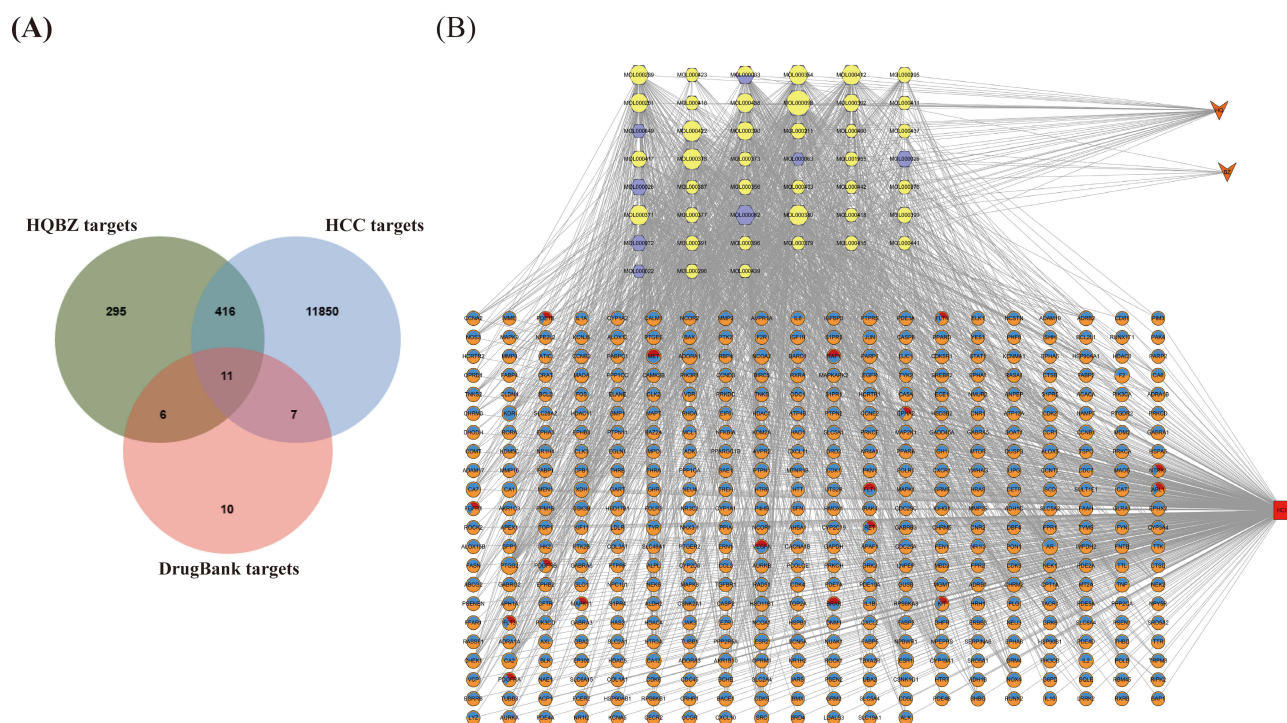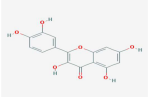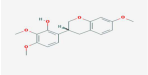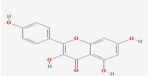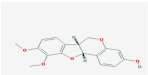
(A)　　　　　　　　　　(B)

Figure 1 HQBZ-Compound-Target-HCC complex network. (**A**) Venn diagrams of the common targets of *Astragalus–Atractylodes* herb pair (HQBZ), hepatocellular carcinoma (HCC), and FDA-approved drug for HCC. (**B**) HQBZ-Compound-Target-HCC complex network, including 481 nodes with 2159 edges. The V-shaped nodes represent *Astragalus* (HQ) and *Atractylodes* (BZ), the hexagonal nodes represent 45 candidate bioactive ingredients of HQ and BZ (yellow and purple represent the bioactive ingredients from HQ and BZ, respectively). Round nodes represent 433 putative targets for HCC treatment using HQBZ (red is the target of action from FDA-approved drug for HCC, blue is the target of HQBZ, Orange is the target of HCC), and red square nodes represent HCC.
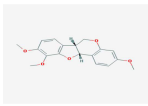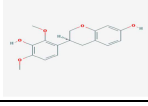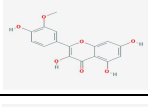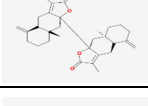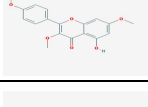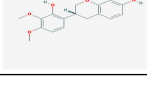
performed on the network. Finally, we obtained the 7 key targets of HQBZ in the treatment of HCC according to the top 5% of CC, including GAPDH (CC=0.69), EGFR (CC=0.67), SRC (CC=0.65), ESR1 (CC=0.65), TNF (CC=0.63), IL6 (CC=0.61), and JUN (CC=0.61).

Table 1 Top ten Compounds Information of HQBZ-Compound-Target-HCC Network

Mol ID	Molecule Name	Molecule Structure	OB (%)	DL	Degree
MOL000098	Quercetin		46.43	0.28	140
MOL000378	7-O-methylisomucronulatol		74.69	0.3	92
MOL000422	Kaempferol		41.88	0.24	90
MOL000380	(6aR,11aR)-9,10-dimethoxy-6a,11a-dihydro-6H-benzofurano[3,2-c] chromen-3-ol		64.26	0.42	87

(Continued)

Table 1 (Continued).

Mol ID	Molecule Name	Molecule Structure	OB (%)	DL	Degree
MOL000371	3,9-di-O-methylnissolin		53.74	0.48	84
MOL000412	Mucronulatol		4.22	0.26	84
MOL000354	Isorhamnetin		49.6	0.31	78
MOL000062	Biatractylolide		17.45	0.81	77
MOL000239	Jaranol		50.83	0.29	76
MOL000438	(3R)-3-(2-hydroxy-3,4-dimethoxyphenyl)chroman-7-ol		67.67	0.26	72

Transcriptional Regulatory Network Construction and Analysis

To explore the mechanism of HCC treatment using HQBZ at the transcriptome level, the transcriptional regulation network data of the human genome were downloaded from the TRRUST database.[16] A total of 71 TF genes from HQBZ and 1166 non-TF genes from HCC were identified. The HQBZ–HCC transcriptional regulatory network with 1237 nodes and 1405 edges was built using data entered into the Cytoscape 3.7.2 program (Figure 3A). The network was subjected to topology analysis, and nodes with a greater than average degree were retained to obtain a subnetwork with 282 nodes and 1074 edges (Figure 3B). In the subnetwork, 59 nodes were derived from the TF genes of HQBZ, indicating that 59 transcription factors from HQBZ regulated most non-TFs in HCC. In this subnetwork, the top 5% TF genes with degrees were RELA (degrees=210), TP53 (degrees=121), and STAT3 (degrees=100). In our opinion, these three targets are significant HQBZ-regulated transcription factors in HCC that play critical roles in the transcriptional regulatory network.

GO Biofunctional Enrichment and KEGG Signaling Pathway Analysis

To further explore the biological mechanism of HQBZ in HCC prevention and treatment, GO and KEGG analyses were performed on the 140 targets and 59 transcription factors obtained from the network analysis. The 188 targets obtained were entered into the Metascape platform[17] for GO analysis. In total, 1872 BP items were enriched (p≤0.01), including regulation of apoptotic signaling pathway, regulation of T-cell activation and programmed cell death. Moreover, 121 CC, including membrane rafts, membrane microdomains, and chromosomal regions, were screened. Finally, 201 MF items, including protein serine/threonine kinase activity, NF-κB binding, and STAT family protein binding, were screened. Figure 4A shows the top 15 items in each of the three considerably rich GO analysis types. A similar technique was used to enrich 187 KEGG pathways (p<0.01). The signaling pathways closely related to HCC, including the HCC, T-cell receptor signaling pathway, PD-L1 expression and PD-1 checkpoint pathway in cancer, and the JAK-STAT signaling pathway, are shown in Figure 4B.
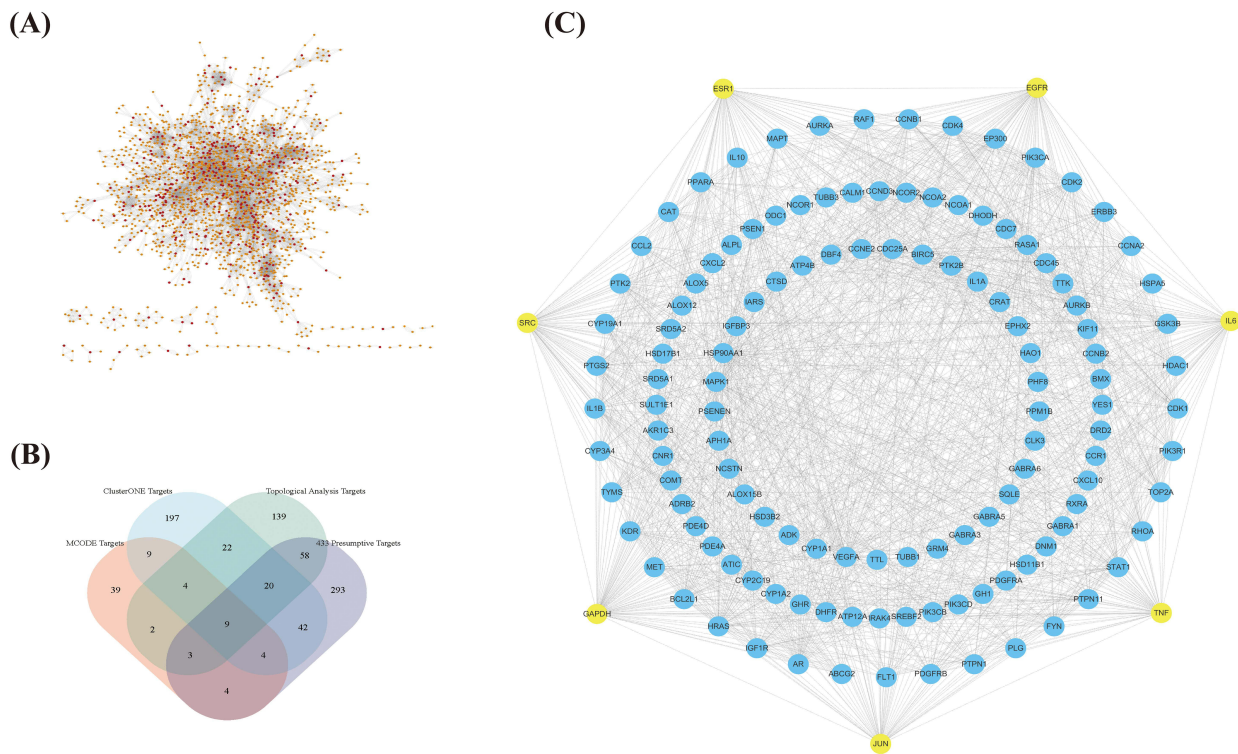
(A)

(B)

(C)

Figure 2 Protein–protein interaction (PPI) network analysis of *Astragalus–Atractylodes* herb pair (HQBZ)–hepatocellular carcinoma (HCC). (**A**) PPI network of HQBZ in the treatment of HCC, including 2165 nodes with 20,797 edges. Red and Orange nodes represent 408 HQBZ targets on HCC and 1757 interacting targets collected from the STRING database, respectively. (**B**) Intersection of topological analysis, MCODE cluster analysis, ClusterONE cluster analysis target and HQBZ to HCC therapeutic target. (**C**) The PPI subnetwork of HQBZ against HCC targets consisted of 133 nodes and 1491 edges. Yellow nodes indicate the important potential targets for HCC prevention and treatment using HQBZ.
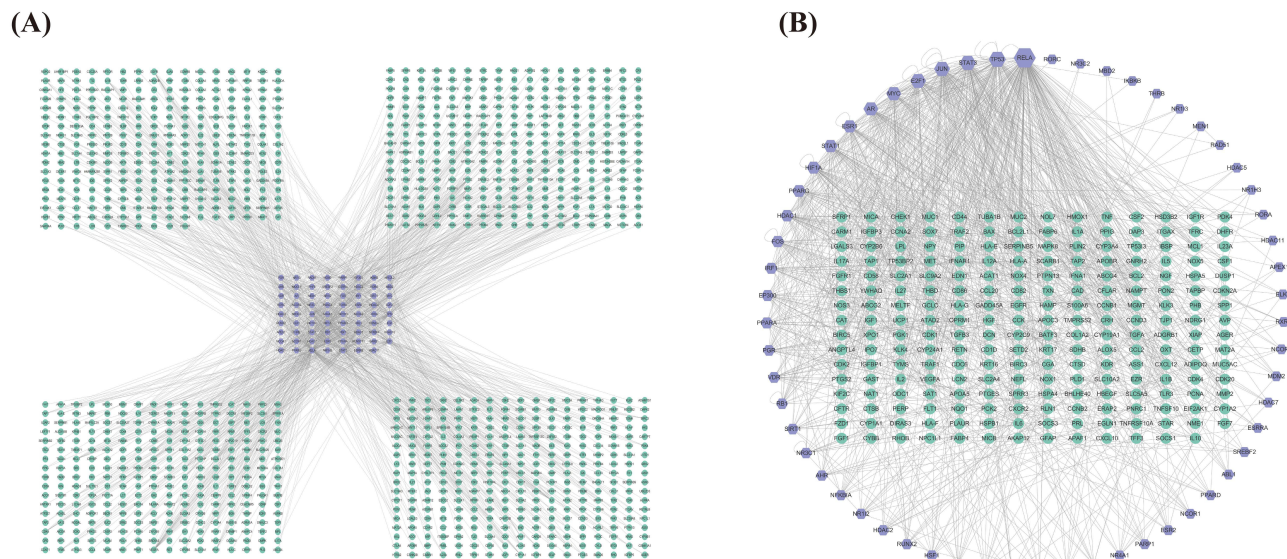
(A)

(B)

Figure 3 Analysis of transcriptional regulatory network of *Astragalus–Atractylodes* herb pair (HQBZ)–hepatocellular carcinoma (HCC). (**A**) The HQBZ–HCC transcriptional regulatory network consisted of 1237 nodes and 1405 edges. The green circular and purple hexagonal nodes represent 1166 non-TF genes of HCC and 71 TF genes of HQBZ, respectively. (**B**) A subnetwork of the HQBZ–HCC transcriptional regulatory network consisting of 282 nodes and 1074 edges. A big purple hexagon node indicates a high degree of the TF genes of HQBZ.
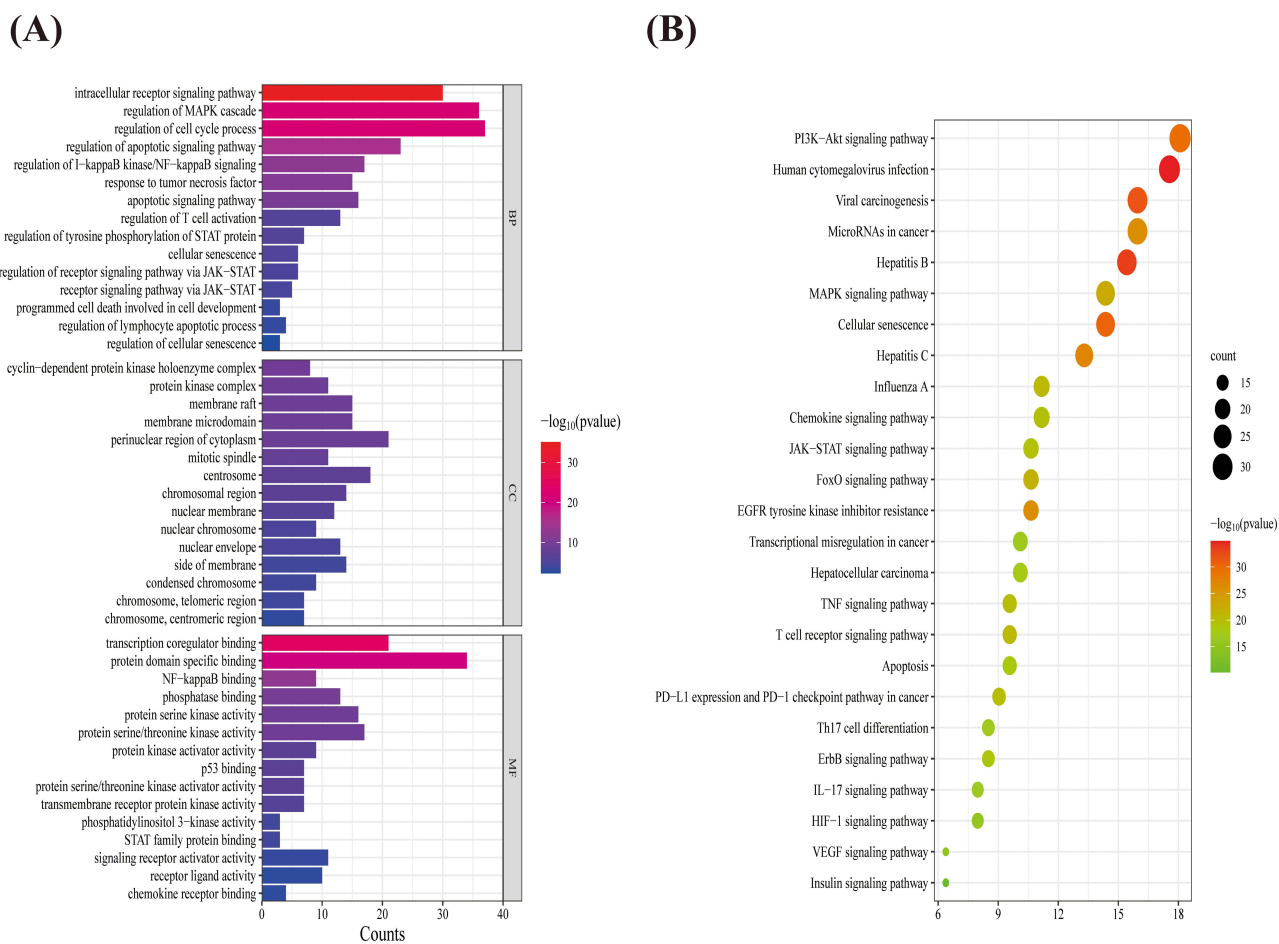
(A)

(B)

Figure 4 Enrichment analysis using GO and KEGG with presumed targets. (**A**) GO analysis was performed using the Metascape database. In total, 1872 biological processes (BP), 121 cell components (CC), 201 molecular functions (MF) were enriched, while 15 enrichment results are presented. (**B**) The KEGG analysis was carried by using the Metascape database. Out of the 187 enriched KEGG pathways, the top 25 pathways are displayed.

In addition, the outcomes of GO and KEGG analyses showed that HQBZ targets for HCC were significantly enriched in T-cell-related signaling pathways and programmed cell death signaling pathways, implying that the anti-HCC action of HQBZ might be connected to programmed cell death control.

Molecular Docking Verification

The seven key targets of HQBZ for HCC prevention and treatment were integrated with three important transcription factors for HCC transcriptional regulation, and molecular docking was performed with 10 important active compounds of HQBZ for HCC prevention and treatment. GAPDH, EGFR, SRC, ESR1, TNF, IL6, JUN, RELA, TP53, and STAT3 crystal structures are 6YND, 8A27, 7NG7, 7UJO, 6I50, 5SFK, 5I2L, 7BIW, 8HKW, and 6SM8, respectively. The binding energies of the ligand and receptor are shown in Figure 5A. Proteins and ligands can form a stable bond if the binding energy score is less than −5 kcal/mol. The results showed that all targets stably bind to the active compounds, among which EGFR, RELA, and IL6 had the strongest binding activity, and biatractylolide had the strongest binding activity with these three targets. EGFR and RELA bind to biatractylolide via two amino acid residues (ARG-841/ARG-803 and LYS-214/THR-217, respectively). IL-6 binds to biatractylolide via one amino acid residue (SER-573). The docking results were visualized in 3D form (Figure 5B−D).

It is noteworthy that the IL-6/STAT3 signaling pathway is a classical tumor signaling pathway that has many effects on tumor cell proliferation, survival, invasion, and metastasis, as well as the inhibition of antitumor immunity.[22] IL-6 forms an IL-6/IL-6R/gp130 complex with membrane-bound gp130 and IL-6R, which activates JAK and STAT3

(A)

(B)

EGFR act on Biatractylolide（Affinity=-9.4 kcal/mol）

(C)

RELA act on Biatractylolide（Affinity=-9.2 kcal/mol）

(D)

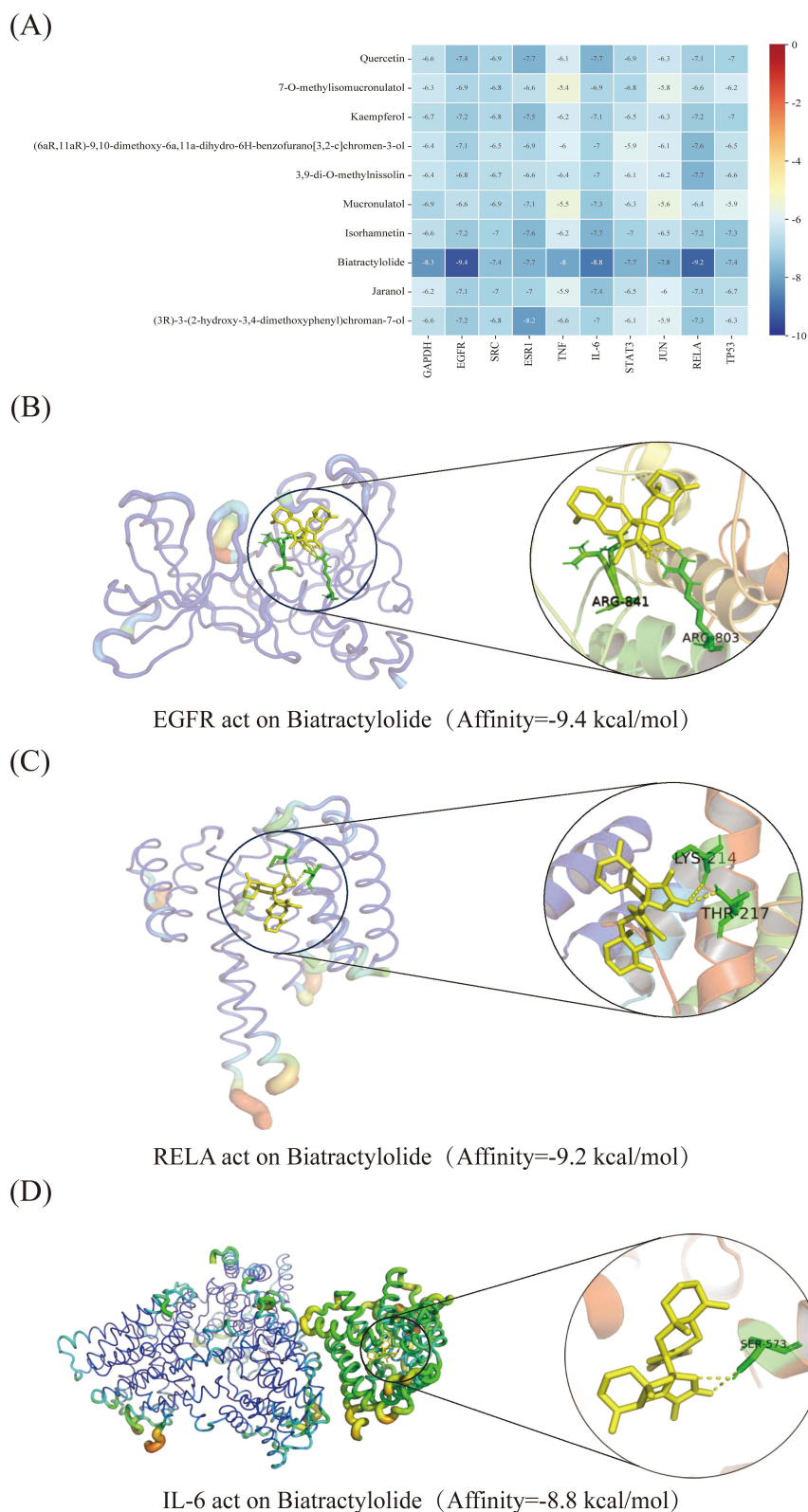IL-6 act on Biatractylolide（Affinity=-8.8 kcal/mol）

Figure 5 Molecular docking verification of postulated components and key targets. (**A**) The heat map displays 100 pairings of molecular docking results. (**B–D**) Combined the three most active docking pairs, biatractylolide with EGFR, biatractylolide with RELA, and biatractylolide with IL-6, and three-dimensional docking results are shown.

phosphorylation. IL-6 and STAT3 are the core targets of our discovery, and JAK/STAT signaling pathway is an important signaling pathway enriched by us. Therefore, we speculate that the IL-6/STAT3 signaling pathway is probably the main signaling mechanism used in HQBZ therapy for HCC.

HQBZ Regulates IL-6/STAT3 Signal Transduction in Mouse Spleen Cells in vitro and Improves CD8$^+$T Cell Ratio

Previous studies have demonstrated that patients with HCC have significantly higher serum IL-6 levels than individuals without HCC[23,24] and HCC prognosis worsens with high serum IL-6 level,[25] which further supports the results of our network pharmacology analysis; thus, IL-6 might be a crucial target for treating HCC with HQBZ. To test whether HQBZ can regulate the IL-6/STAT3 signaling pathway, we stimulated the spleen cells of healthy mice with recombinant murine IL-6 to activate the IL-6/STAT3 signaling pathway. We also paid special attention to the regulatory effects of HQBZ on T cells, the CD4$^+$ and CD8$^+$T cells proportions were measured by flow cytometry for all groups (Figure 6A). Adding recombinant murine IL-6 significantly reduced the CD8$^+$T-cell proportion in the IL-6 group compared to that in the control group, whereas adding HQBZ drug-containing serum hardly harmed CD8$^+$T cells in the HQBZ group. Interestingly, HQBZ administration significantly restored the CD8$^+$T-cell levels in the IL-6+HQBZ group compared with those in the IL-6 group, whereas IL-6+Solvent group administration did not improve CD8$^+$T-cell levels. However, the percentage of CD4$^+$T cells did not differ significantly across the groups, suggesting that HQBZ regulates T cells mainly by regulating CD8$^+$T cells rather than CD4$^+$T cells.

Furthermore, the expression levels of the IL-6/STAT3 signaling pathway-related proteins, IL-6R, p-STAT3, and c-MAF, in CD8$^+$T cells were detected by flow cytometry. HQBZ significantly inhibited the recombinant murine IL-6-induced IL-6/STAT3 signaling pathway in CD8$^+$T cells, thus restoring IL-6R expression and downregulating p-STAT3 and c-MAF expression (Figure 6B). CD8$^+$T cells in mice is consists of three major subsets that can be marked by using CD44 and CD62 antibodies: naïve T cell (Tn; CD44$^-$CD62$^+$), central memory T cell (Tcm; CD44$^+$CD62L$^+$), and effector/memory T cell (Tem; CD44$^+$CD62L$^-$)。We further detected the expression level of IL-6R in the subsets of CD8$^+$T cells in each group, and the results showed that the use of IL-6 significantly reduced the expression level of IL-6R in the subsets of CD8$^+$T cells, while HQBZ eliminated the effect of IL-6 and significantly restored the expression level of IL-6R (Figure 6C).

HQBZ Alleviates T Cell Exhaustion Caused by IL-6, Restores Cytotoxicity of Exhausted T Cells and Delays Apoptosis

Strong expression of immunosuppressive receptors, particularly PD-1, TIGIT, TIM-3, and LAG-3, is characteristic of T-cell exhaustion.[26] Studies have confirmed that CD8$^+$T cells are depleted in patients with HCC,[27] and CD8$^+$T-cell exhaustion worsens their progression-free survival(PFS) and overall survival(OS).[2] KEGG enrichment analysis suggested that HQBZ treatment of HCC was related to PD-L1 expression and PD-1 checkpoint pathway in cancer pathway Therefore, flow cytometry was used to detect the expression of immunosuppressive receptors including PD-1, TIGIT, TIM-3 and LAG-3 on CD8$^+$T cells in each group (Figure 7A). The percentage of PD-1$^+$CD8$^+$, TIGIT$^+$CD8$^+$, TIM-3$^+$CD8$^+$ and LAG-3$^+$CD8$^+$T cells were significantly high in the IL-6 group, indicating that IL-6 causes CD8$^+$T-cell exhaustion. These findings demonstrate that HQBZ treatment downregulates immunosuppressive receptors expression in the HQBZ+IL-6 group, suggesting that HQBZ can reverse CD8$^+$T cell depletion.

The exhausted T cells also show various dysfunctions such as increased apoptosis, decreased proliferation capacity, and weakened killing function.[28] Therefore, we further detected Annexin V and Ki67 expression levels in CD8$^+$T cells to indicate apoptosis and proliferation, detected the expression of perforin and GranzymeB to indicate the killing effect (Figure 7B). The results showed that the apoptosis level of CD8$^+$T cells in IL-6 group was significantly increased, and the proliferation and killing ability were significantly decreased, indicating the dysfunction of CD8$^+$T cells. HQBZ successfully alleviated and reduced dysfunction, significantly reduced the apoptotic function of exhausted CD8$^+$T cells and improved their proliferation and killing ability.
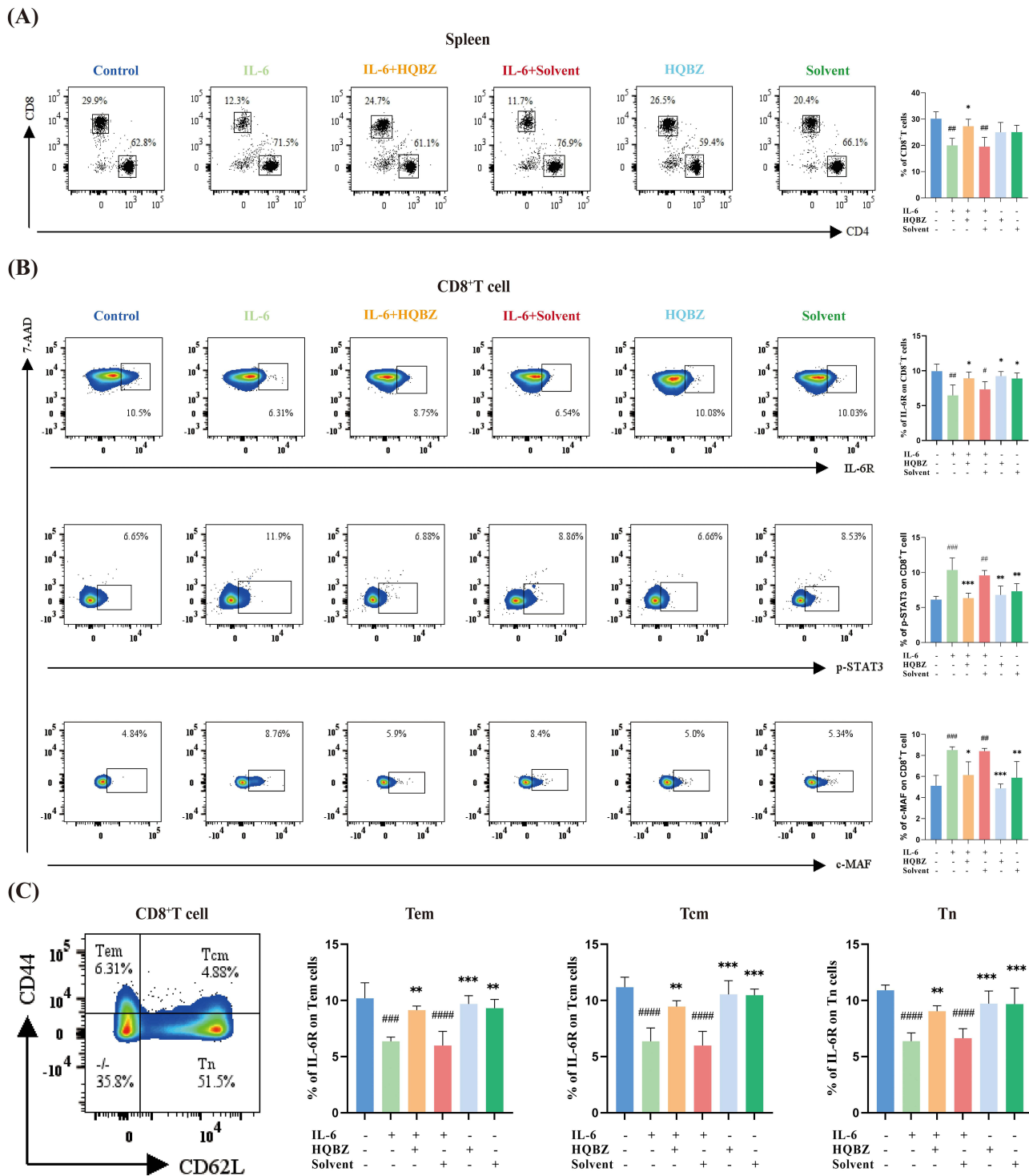
Figure 6 *Astragalus–Atractylodes* herb pair (HQBZ) restored the CD8+T-cell ratio and greatly reduced the interleukin IL-6/STAT3 signaling produced by recombinant murine IL-6. (**A**) The proportion of CD4+ and CD8+T cells in all group was ascertained via flow cytometry, and statistical analysis was carried out. (**B**) Flow cytometry was used to detect and statistically assess the IL-6R, p-STAT3, and c-MAF expression in CD8+T cells in all groups. (**C**) Representative plots showing CD44 and CD62L antibody marked CD8+T cell subsets and statistical analysis of the percentage of IL-6R in each subset. Data are expressed as SD ± average (experiments in the study were performed in triplicate). Compared with the control group, #p<0.05, ##p<0.01, ###p<0.001, ####p<0.0001; compared with the IL-6 group, *p<0.05, **p<0.01, ***p<0.001.

HQBZ Upregulates the Exhausted CD8+T Cell Immunostimulatory Factor Level

Another important manifestation of T-cell depletion is changes in immune factors, manifested by reduced expression of proinflammatory factors such as IL-2, IFN-γ, TNF-α, these changes decrease or even lose the antitumor ability of T cells.
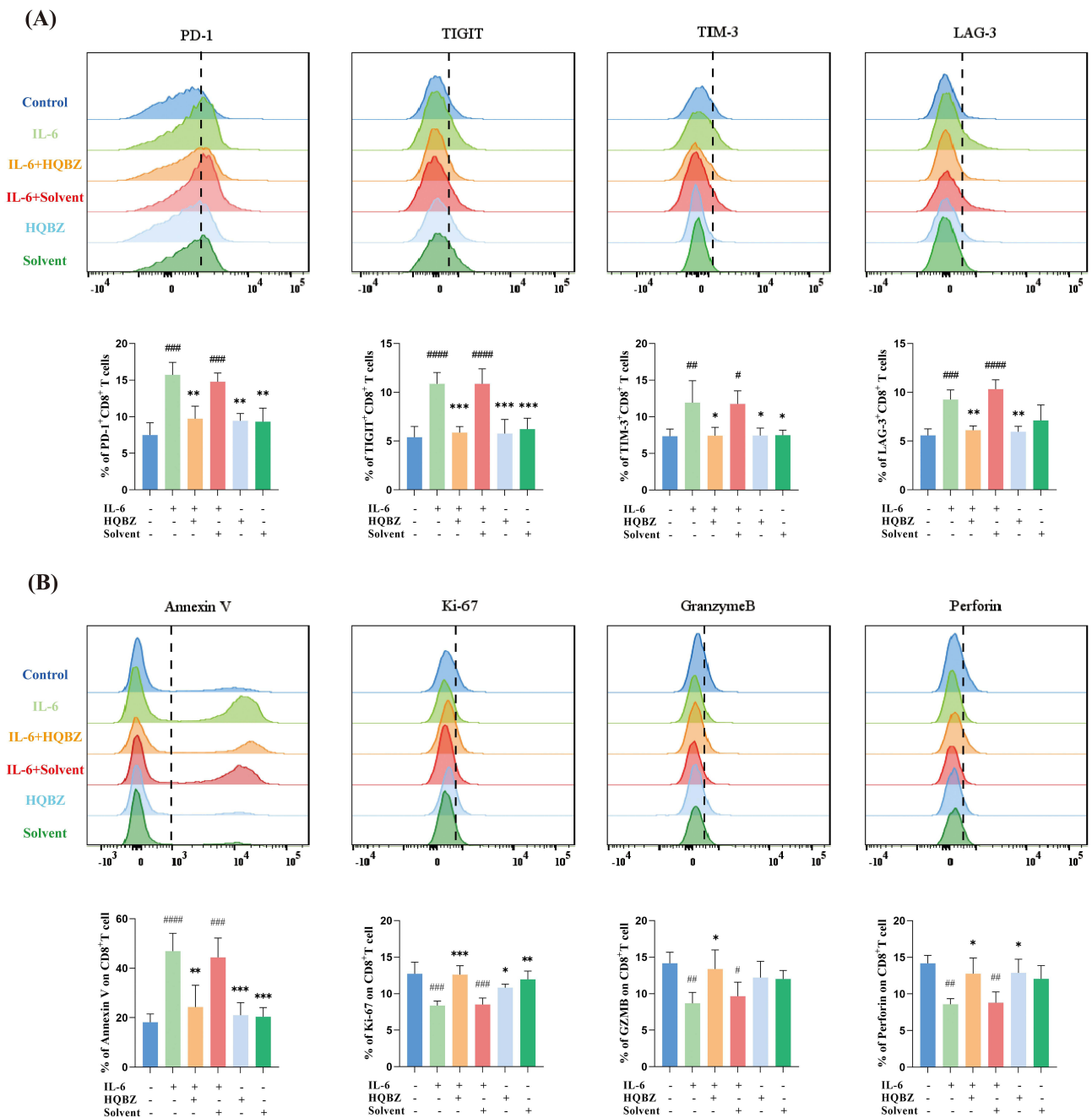
Figure 7 *Astragalus–Atractylodes* herb pair (HQBZ) alleviates the exhaustion phenotype of CD8$^+$T cells, improves the proliferation ability and killing function of exhausted CD8$^+$T cells, and reduces the apoptosis level. (**A**) Flow cytometry was used to detect the proportion of immunosuppressive receptors, including PD-1, TIGIT, TIM-3, and LAG-3, of CD8$^+$T cells in each group. (**B**) Detecting the expression of Annexin V, Ki67, Perforin, and GranzymeB in CD8$^+$T cells of each group by Flow cytometry. Data are expressed as SD± average (experiments in the study were performed in triplicate). Compared with the control group, $^{\#}p < 0.05$, $^{\#\#}p < 0.01$, $^{\#\#\#}p < 0.001$, $^{\#\#\#\#}p < 0.0001$; compared with the IL-6 group, $^{*}p < 0.05$, $^{**}p < 0.01$ $^{***}p < 0.001$.

To further observe whether HQBZ can regulate the T-cell immune cytokine production, IL-2, IFN-γ, TNF-α, secretion by CD8$^+$T cells in all groups was measured by flow cytometry (Figure 8A−D). Compared with those in the control group, IL-2, IFN-γ, and TNF-α expression levels decreased in the IL-6 group. As expected, compared with that in the IL-6 group, the IL-2, IFN-γ, and TNF-α production increased in the HQBZ+IL-6 group after HQBZ addition. This showed that HQBZ ameliorated the decreased antitumor ability of CD8$^+$T cells induced by IL-6 and restored their antitumor function.
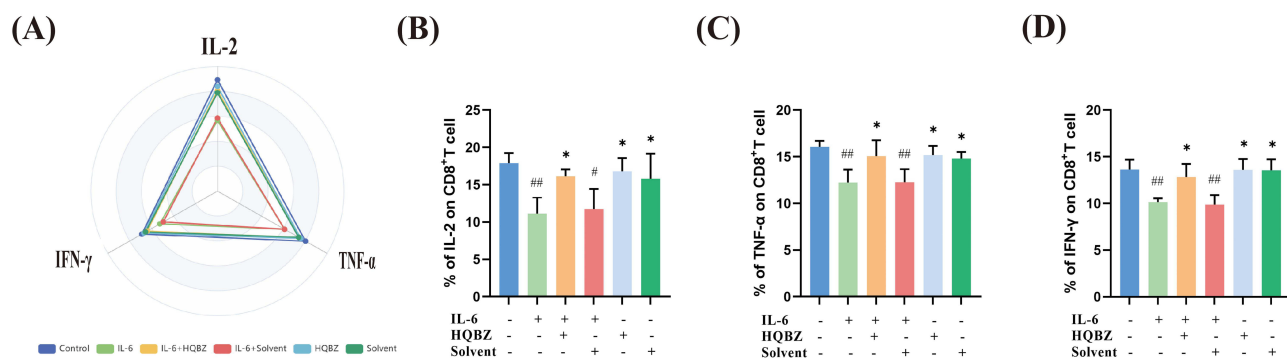
Figure 8 *Astragalus–Atractylodes* herb pair (HQBZ) controls the generation of immune cytokines from CD8^{+}T cells. (**A**) Radar map showing the proportions of IL-2, IFN-γ and TNF-α of CD8^{+}T cells in each group. (**B–D**) The statistical results of IL-2, TNF-α and IFN-γ and percentages of CD8^{+}T cells in each group. Data is expressed as SD± average (experiments in the study were performed in triplicate). Compared with the control group, #p<0.05, ##p<0.01; compared with the IL-6 group, *p<0.05.

HQBZ Regulates IL-6/STAT3 Signaling in Tumor Tissue of H22 Tumor-Bearing Mice, Increasing Tumor-Infiltrating CD8^{+}T Cells

It has been proved that HQBZ is very effective in the treatment of H22 tumor-bearing mice. HQBZ treatment effectively restored the weight of tumor-bearing mice and reduced the weight of tumors, and this therapeutic effect is dose-dependent (Figure S2). To ascertain whether HQBZ acts as a therapeutic agent for HCC via the IL-6/STAT3 signaling pathway, we assessed the regulatory function of HQBZ in the IL-6/STAT3 signaling pathway using an H22 tumor-bearing mouse model. The expression of STAT3 in tumor tissues was determined through immunohistochemistry, and the results showed that the expression of STAT3 in tumor tissue decreased significantly after HQBZ treatment (Figure 9A and B). The degree of CD8^{+}T cell infiltration, the expression of IL-6, STAT3, and c-MAF, a downstream component of IL-6/STAT3 signal transduction, in tumor tissues, were determined through immunofluorescence. The proportion of tumor-infiltrating CD8^{+}T cells increased after HQBZ treatment, whereas the expression of IL-6, STAT3, and c-MAF decreased significantly, indicating that HQBZ can downregulate the expression of IL-6 in tumor tissues and significantly regulate IL-6/STAT3 signaling in tumors. Subsequently, we further detected the expression of STAT3 and c-MAF on CD8^{+}T cells, and the results showed that the expression of STAT3 and c-MAF on CD8^{+}T cells was also significantly inhibited by HQBZ (Figure 9C–E).

Discussion

The proportions of new cases and deaths from HCC are 45.3% and 47.1% in China.[29] Although various clinical treatments have been used to treat HCC, the mortality rate of patients with HCC remains high, the 5-year survival rate of patients with HCC in China is only 12.1%.[30] Currently, T-cell-based immunotherapy is widely used clinically. Immune checkpoint inhibitors (ICIs) targeting CTLA4, PD-1, and PD-L1 have been approved by the FDA and shown excellent therapeutic effect in clinic.[31–33] However, with the continuous expansion of ICI use, immune-related adverse events (irAEs) caused by ICI are increasingly emerging.[34] TCM is known for its holistic approach and compounds that simultaneously regulate many targets are abundant in Chinese herbs. In this context, HCC treatment has garnered increasing attention owing to the growing emphasis on TCM. As a classic herbal pair, in recent years, several studies have shown that HQBZ has substantial anticancer effects and can effectively improve the tumor immune microenvironment.[35–39] Nevertheless, the exact mechanism of action of HQBZ in HCC treatment remains uncertain, and its role and potential anti-HCC mechanism are worthy of further study. In this study, network pharmacological analysis and molecular docking methods were used to explore the target and signal pathway of HQBZ in the treatment of HCC. The mechanism of HQBZ in the treatment of HCC was further verified by multi-color flow cytometry, immuno-histochemistry and immunofluorescence in vivo and in vitro.

This study primarily aimed to examine the possible mechanism of action of HQBZ in the treatment of HCC. The HQBZ-Compound-Target-HCC composite network was used to further explore the core components. Through network
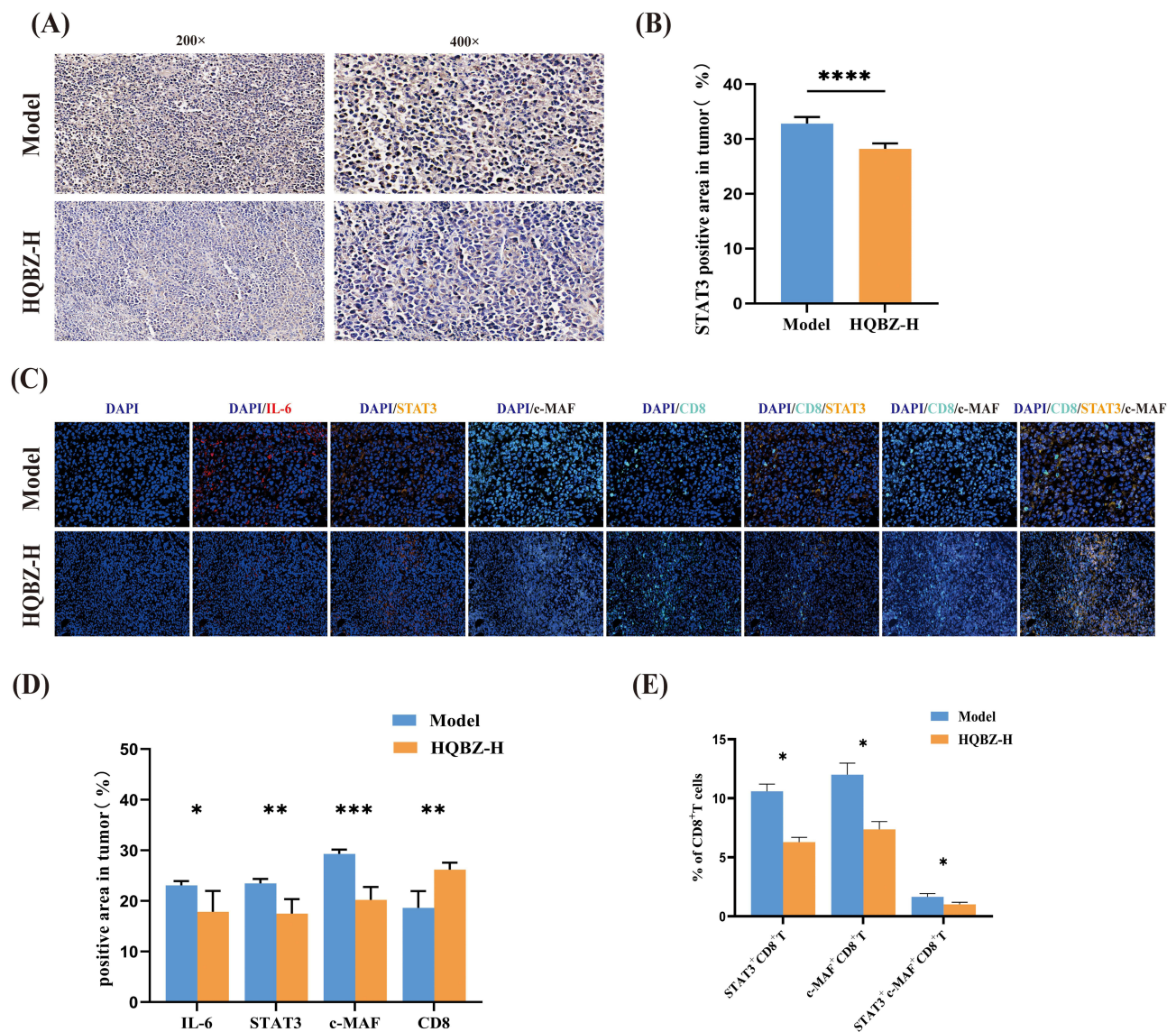
Figure 9 *Astragalus–Atractylodes* herb pair (HQBZ) augmented the degree of infiltration of CD8+T cells within the tumor tissues, resulting in a notable decrease in the expression of IL-6, STAT3, and c-MAF in tumor tissue and CD8+T cells. (**A** and **B**) immunohistochemical detection of the effect of HQBZ on the expression of STAT3 in tumor tissues and quantitative analysis (200× and 400× magnification). (**C–E**) Immunofluorescent detection and quantitative analysis of the effect of HQBZ on the expression of IL-6, STAT3, and c-MAF in tumor tissue and CD8+T cells. n=1 per group for histological staining. Compared with the model group, *p<0.05, **p<0.01, ***p<0.001, ****p<0.0001.

analysis, 10 core components, including biatractylolide, quercetin, kaempferol, and isorhamnetin, that are crucial to the network and closely linked to other targets and active constituents were identified. In vitro experiments have shown that biatractylolide has antioxidant activity, which can reduce the release of the apoptotic component cytochrome c and reactive oxygen species (ROS).[40] Quercetin reduces the expression of key components of the tumor microenvironment (TME) and ABCC3, thereby inhibiting the growth of early HCC tumors.[41] In addition, quercetin targets Notch and Hh signaling pathways, regulates apoptosis and proliferation, and plays an anti-HCC role.[42] Kaempferol protects liver parenchymal cells through antioxidant and anti-apoptotic mechanisms, inhibits endoplasmic reticulum stress, and inhibits tumor growth.[43] Isorhamnetin inhibits the epithelial−mesenchymal transition (EMT) and tumor progression by inhibiting the deubiquitination of USP7 to YY1 in HCC.[44] Numerous prior studies have indicated that these elements could potentially be the primary active ingredients in HQBZ for HCC; therefore, they are worthy of further study.

PPI and HQBZ−HCC transcriptional regulatory networks were used to identify the main targets of HQBZ in HCC. PPI network analysis showed that GAPDH, EGFR, SRC, ESR1, TNF, IL6, and JUN were core targets. Studies have shown that GAPDH accelerates HCC development by upregulating PHGDH to increase histone methylation levels and promote the transformation from glycolysis to serine biosynthesis.[45] Previous studies have confirmed that Lenvatinib efficacy in HCC is decreased by EGFR activation and that an EGFR inhibitor combined with Lenvatinib therapy has a powerful antitumor cell proliferation effect.[46] Weng et al have indicated that silencing SRC reduces STAT3/NF-κB signaling and enhances radiosensitivity of HCC.[47] Jeon et al have found that patients with HCC expressing Erα (encoded by ESR1) had better overall and disease-free survival periods.[48] Moreover, obesity-induced increases in TNF and IL-6 expression activate STAT3, thereby promoting HCC development.[49] In addition, fibronectin 1 (FN1) derived from tumor-associated macrophages and fibroblasts promotes HCC metastasis through the JUN pathway.[50] Analysis of the HQBZ−HCC transcriptional regulatory network showed that RELA, TP53, and STAT3 are the core transcription factors of HQBZ that regulate HCC transcription. RELA (NF-κB p65) is an important member of the NF-κB family, and inhibiting NF-κB p65 phosphorylation can inhibit HCC.[51] TP53 is a tumor suppressor gene, and an organoid-based study has shown that TP53 knockout leads to the loss of tumor suppressor function, leading to tumorigenesis.[52] STAT3, a cancer-promoting transcription factor, can be activated by IL-6-mediated tumor-stromal crosstalk to promote HCC progression.[53–55] Based on previous research results and considering the results of the network pharmacological analysis, the above 10 core targets play a major role in HCC occurrence and development, and they are trustworthy as possible therapeutic targets of HQBZ for HCC.

According to our findings in network pharmacology studies, the above 10 core compounds were subjected to molecular docking with seven core targets and three core transcription factors to verify our network pharmacological prediction results. According to the docking data, each compound bound to the proteins. In particular, the most stable binding of the three pairs of small-molecule ligands and large-molecule protein receptors was observed for biatractylolide and EGFR, RELA, and IL-6. Simultaneously, we observed that the DL value of biatractylolide was 0.81, which was the highest among the 10 core compounds, indicating that biatractylolide had the highest similarity to known drugs and was the most likely compound to become a drug.

IL-6 activates the STAT3 pathway and participates in hepatitis B-related HCC development.[54] In addition, T-cell immunological modulation is significantly influenced by the IL-6/STAT3 signaling pathway, and endogenous TIM-3 expression in tumor cells promotes liver cancer development through the NF-κB/IL-6/STAT3 axis.[55] The results of network pharmacological analysis and GO and KEGG pathway enrichment analysis were comprehensively verified by our experiments, which established that HQBZ can inhibit IL-6/STAT3 signaling pathway transduction, increase tumor-infiltrating CD8$^+$T cells, reverse T cell exhaustion and restore T cell immune function. Specifically, HQBZ can restore IL-6R levels, down-regulate the expression of STAT3 and c-MAF in IL-6/STAT3 signaling pathway, up-regulate the proportion of CD8$^+$T cells and decreased the production of T cell immunosuppressor receptors such as PD-1, TIGIT, TIM-3, LAG-3. Moreover, the immunostimulatory factors IL-2, IFN-γ and TNF-α were increased, and the tumor immunosuppressive microenvironment was improved. It can also down-regulate T cell apoptosis, restore T cell proliferation and killing ability, the immune function of exhausted CD8$^+$T cells was restored.

This study has some limitations. First, the regulatory effect of HQBZ on T-cell immunosuppressive receptors and immune factor expression levels has only been validated in vitro and has not been examined in H22 tumor-bearing mice. Second, this study conducted further experimental verification based on network pharmacology studies and only clarified some of the targets and mechanisms of HQBZ anti-HCC. Finally, this study did not use inhibitors to further verify the IL-6/STAT3 signaling pathway. Therefore, future studies should use in vivo models and human samples to fully validate the efficacy and mechanisms of HQBZ.

Conclusion

This investigation verified that biatractylolide is a crucial component of HQBZ for HCC treatment and primarily targets EGFR, RELA, and IL-6. Moreover, HQBZ regulates IL-6/STAT3 signaling pathway transduction, regulates programmed cell death, increase tumor-infiltrating CD8$^+$T cells, alleviates T-cell exhaustion, improve immunosuppressive microenvironment, and restore T cell immune function. The mechanism may be realized through IL-6/STAT3 signaling pathway to

play a therapeutic role in HCC. These findings provide trustworthy evidence of the efficacy of TCM in treating HCC and suggest reliable candidate ingredients for future drug development.

Abbreviations

AUC, area under the curve; LS, least squares; NE, not estimable; HQ, *Astragalus* (Chinese name: Huangqi); BZ, *Atractylodes* (Chinese name: Baizhu); HCC, hepatocellular carcinoma; TCM, traditional Chinese medicine; PPI, protein–protein interaction; BC, betweenness centrality; CC, closeness centrality; ASPL, average shortest path length; BP, biological process; CC, cell components; MF, molecular function; Tn, naïve T cell; Tcm, central memory T cell; Tem, effector/memory T cell; PFS, progression-free survival; OS, overall survival; ICIs, Immune checkpoint inhibitors; irAEs, immune-related adverse events; YFJP, Yangyin Fuzheng Jiedu prescription; ROS, reactive oxygen species; TME, the tumor microenvironment; EMT, epithelial−mesenchymal transition; EMT, epithelial−mesenchymal transition; FN1, fibronectin 1.

Ethical Statement

The human dataset GSE62232 used in this study is open source data, the dataset has been approved by institutional review board committees (CCPRB Paris Saint-Louis, 1997, 2004, and 2010, approval number 01-037; Bordeaux 2010-A00498-31). Written informed consent was obtained in accordance with French legislation.

The use of experimental animals was in conformance with the Animal Ethics Committee of the Animal Care and Use Committee of Beijing University of Chinese Medicine and strictly operated according to the Guide for the Care and Use of Laboratory Animals published by the US National Institutes of Health, strictly abide by the "Five F" and the "Three R" principle. (License no. BUCM-4-2,021,062,301-2067).

Author Contributions

All authors made a significant contribution to the work reported, whether that is in the conception, study design, execution, acquisition of data, analysis and interpretation, or in all these areas; took part in drafting, revising or critically reviewing the article; gave final approval of the version to be published; have agreed on the journal to which the article has been submitted; and agree to be accountable for all aspects of the work.

Disclosure

The authors declare that the research was conducted in the absence of any commercial or financial relationships that could be construed as a potential conflict of interest.

References

1. Sung H, Ferlay J, Siegel RL, et al. Global cancer statistics 2020: GLOBOCAN estimates of incidence and mortality worldwide for 36 cancers in 185 countries. *CA Cancer J Clin*. 2021;71(3):209–249. doi:10.3322/caac.21660
2. Barsch M, Salie H, Schlaak AE, et al. T-cell exhaustion and residency dynamics inform clinical outcomes in hepatocellular carcinoma. *J Hepatol*. 2022;77(2):397–409. doi:10.1016/j.jhep.2022.02.032
3. Huang H, Fang J, Fan X, et al. Advances in Molecular Mechanisms for Traditional Chinese Medicine Actions in Regulating Tumor Immune Responses. *Front Pharmacol*. 2020;11:1009. doi:10.3389/fphar.2020.01009

4. Liu YX, Bai JX, Li T, et al. A TCM formula comprising Sophorae Flos and Lonicerae Japonicae Flos alters compositions of immune cells and molecules of the STAT3 pathway in melanoma microenvironment. *Pharmacol Res*. 2019;142:115–126. doi:10.1016/j.phrs.2019.02.020

5. Wang H, Wei L, Mao D, et al. Combination of oxymatrine (Om) and astragaloside IV (As) enhances the infiltration and function of TILs in triple-negative breast cancer (TNBC). *Int Immunopharmacol*. 2023;125(Pt A):111026. doi:10.1016/j.intimp.2023.111026

6. Nogales C, Mamdouh ZM, List M, Kiel C, Casas AI, Schmidt H. Network pharmacology: curing causal mechanisms instead of treating symptoms. *Trends Pharmacol Sci*. 2022;43(2):136–150. doi:10.1016/j.tips.2021.11.004

7. Barrett T, Wilhite SE, Ledoux P, et al. NCBI GEO: archive for functional genomics data sets--update. *Nucleic Acids Res*. 2013;41(Database issue): D991–D95. doi:10.1093/nar/gks1193

8. Wishart DS, Feunang YD, Guo AC, et al. DrugBank 5.0: a major update to the DrugBank database for 2018. *Nucleic Acids Res*. 2018;46(D1): D1074–D1082. doi:10.1093/nar/gkx1037

9. Ru J, Li P, Wang J, et al. TCMSP: a database of systems pharmacology for drug discovery from herbal medicines. *J Cheminform*. 2014;6(1):13. doi:10.1186/1758-2946-6-13

10. UniProt C, Martin M-J, Orchard S. UniProt: the universal protein knowledgebase in 2021. *Nucleic Acids Res*. 2021;49(D1):D480–D489. doi:10.1093/nar/gkaa1100

11. Kim S, Chen J, Cheng T, et al. PubChem in 2021: new data content and improved web interfaces. *Nucleic Acids Res*. 2021;49(D1):D1388–D1395. doi:10.1093/nar/gkaa971

12. Gfeller D, Grosdidier A, Wirth M, Daina A, Michielin O, Zoete V. SwissTargetPrediction: a web server for target prediction of bioactive small molecules. *Nucleic Acids Res*. 2014;42(Web Server issue):W32–W38. doi:10.1093/nar/gku293

13. Liu H, Wang J, Zhou W, Wang Y, Yang L. Systems approaches and polypharmacology for drug discovery from herbal medicines: an example using licorice. *J Ethnopharmacol*. 2013;146(3):773–793. doi:10.1016/j.jep.2013.02.004

14. Shannon P, Markiel A, Ozier O, et al. Cytoscape: a software environment for integrated models of biomolecular interaction networks. *Genome Res*. 2003;13(11):2498–2504. doi:10.1101/gr.1239303

15. Szklarczyk D, Kirsch R, Koutrouli M, et al. The STRING database in 2023: protein-protein association networks and functional enrichment analyses for any sequenced genome of interest. *Nucleic Acids Res*. 2023;51(D1):D638–D646. doi:10.1093/nar/gkac1000

16. Han H, Cho JW, Lee S, et al. TRRUST v2: an expanded reference database of human and mouse transcriptional regulatory interactions. *Nucleic Acids Res*. 2018;46(D1):D380–D386. doi:10.1093/nar/gkx1013

17. Zhou Y, Zhou B, Pache L, et al. Metascape provides a biologist-oriented resource for the analysis of systems-level datasets. *Nat Commun*. 2019;10 (1):1523.

18. Kitchen DB, Decornez H, Furr JR, Bajorath J. Docking and scoring in virtual screening for drug discovery: methods and applications. *Nat Rev Drug Discov*. 2004;3(11):935–949. doi:10.1038/nrd1549

19. Berman HM, Westbrook J, Feng Z, et al. The Protein Data Bank. *Nucleic Acids Res*. 2000;28(1):235–242. doi:10.1093/nar/28.1.235

20. Hsin KY, Matsuoka Y, Asai Y, et al. systemsDock: a web server for network pharmacology-based prediction and analysis. *Nucleic Acids Res*. 2016;44(W1):W507–W513. doi:10.1093/nar/gkw335

21. Seeliger D, de Groot BL. Ligand docking and binding site analysis with PyMOL and Autodock/Vina. *J Comput Aided Mol Des*. 2010;24 (5):417–422. doi:10.1007/s10822-010-9352-6

22. Johnson DE, O'Keefe RA, Grandis JR. Targeting the IL-6/JAK/STAT3 signalling axis in cancer. *Nat Rev Clin Oncol*. 2018;15(4):234–248.

23. Kong L, Zhou Y, Bu H, Lv T, Shi Y, Yang J. Deletion of interleukin-6 in monocytes/macrophages suppresses the initiation of hepatocellular carcinoma in mice. *J Exp Clin Cancer Res*. 2016;35(1). doi:10.1186/s13046-016-0412-1

24. Chao Y, C-Y W, Kuo C-Y, et al. Cytokines are associated with postembolization fever and survival in hepatocellular carcinoma patients receiving transcatheter arterial chemoembolization. *Hepatol Internat*. 2012;7(3):883–892. doi:10.1007/s12072-012-9409-9

25. Yang H, Kang B, Ha Y, et al. High serum IL-6 correlates with reduced clinical benefit of atezolizumab and bevacizumab in unresectable hepatocellular carcinoma. *JHEP Rep*. 2023;5(4). doi:10.1016/j.jhepr.2023.100672

26. Attanasio J, Wherry EJ. Costimulatory and coinhibitory receptor pathways in infectious disease. *Immunity*. 2016;44(5):1052–1068. doi:10.1016/j. immuni.2016.04.022

27. Zheng C, Zheng L, Yoo JK, et al. Landscape of infiltrating T cells in liver cancer revealed by single-cell sequencing. *Cell*. 2017;169(7):1342–56 e16. doi:10.1016/j.cell.2017.05.035

28. Thommen DS, Schumacher TN. T cell dysfunction in cancer. *Cancer Cell*. 2018;33(4):547–562. doi:10.1016/j.ccell.2018.03.012

29. Rumgay H, Arnold M, Ferlay J, et al. Global burden of primary liver cancer in 2020 and predictions to 2040. *J Hepatol*. 2022;77(6):1598–1606. doi:10.1016/j.jhep.2022.08.021

30. Zeng H, Chen W, Zheng R, et al. Changing cancer survival in China during 2003–15: a pooled analysis of 17 population-based cancer registries. *Lancet Glob Health*. 2018;6(5):e555–e67. doi:10.1016/S2214-109X(18)30127-X

31. Eberhardt J, Santos-Martins D, Tillack AF, Forli S. AutoDock vina 1.2.0: new docking methods, expanded force field, and python bindings. *J Chem Inf Model*. 2021;61(8):3891–3898. doi:10.1021/acs.jcim.1c00203

32. Fu Y, Liu S, Zeng S, Shen H. From bench to bed: the tumor immune microenvironment and current immunotherapeutic strategies for hepatocellular carcinoma. *J Exp Clin Cancer Res*. 2019;38(1):396. doi:10.1186/s13046-019-1396-4

33. Llovet JM, Castet F, Heikenwalder M, et al. Immunotherapies for hepatocellular carcinoma. *Nat Rev Clin Oncol*. 2022;19(3):151–172. doi:10.1038/ s41571-021-00573-2

34. Jing Y, Yang J, Johnson DB, Moslehi JJ, Han L. Harnessing big data to characterize immune-related adverse events. *Nat Rev Clin Oncol*. 2022;19 (4):269–280. doi:10.1038/s41571-021-00597-8

35. Pei T, Dai Y, Tan X, et al. Yupingfeng San exhibits anticancer effect in hepatocellular carcinoma cells via the MAPK pathway revealed by HTS(2) technology. *J Ethnopharmacol*. 2023;306:116134. doi:10.1016/j.jep.2023.116134

36. Fang Gong Y, Hou S, Xu JC, et al. Amelioratory effects of astragaloside IV on hepatocarcinogenesis via Nrf2-mediated pSmad3C/3L transformation. *Phytomedicine*. 2023;117:154903. doi:10.1016/j.phymed.2023.154903

37. Cho WC, Leung KN. In vitro and in vivo anti-tumor effects of Astragalus membranaceus. *Cancer Lett*. 2007;252(1):43–54. doi:10.1016/j. canlet.2006.12.001

38. Bamodu OA, Kuo KT, Wang CH, et al. Astragalus polysaccharides (PG2) ENHANCES the M1 polarization of macrophages, functional maturation of dendritic cells, and T cell-mediated anticancer immune responses in patients with lung cancer. *Nutrients*. 2019;11(10). doi:10.3390/nu11102264

39. Bailly C. Atractylenolides, essential components of Atractylodes-based traditional herbal medicines: antioxidant, anti-inflammatory and anticancer properties. *Eur J Pharmacol*. 2021;891:173735. doi:10.1016/j.ejphar.2020.173735

40. Hu Q, Wang J, Irshad M, et al. Neuroprotective effects of the psychoactive compound biatractylolide (BD) in Alzheimer's disease. *Molecules*. 2022;27(23):8294. doi:10.3390/molecules27238294

41. Reyes-Avendano I, Reyes-Jimenez E, Gonzalez-Garcia K, et al. Quercetin regulates key components of the cellular microenvironment during early hepatocarcinogenesis. *Antioxidants*. 2022;11(2):358. doi:10.3390/antiox11020358

42. Salama YA, El-Karef A, El Gayyar AM, Abdel-Rahman N. Beyond its antioxidant properties: quercetin targets multiple signalling pathways in hepatocellular carcinoma in rats. *Life Sci*. 2019;236:116933. doi:10.1016/j.lfs.2019.116933

43. Xiao X, Hu Q, Deng X, et al. Old wine in new bottles: kaempferol is a promising agent for treating the trilogy of liver diseases. *Pharmacol Res*. 2022;175:106005. doi:10.1016/j.phrs.2021.106005

44. Liu H, Han J, Lv Y, et al. Isorhamnetin and anti-PD-L1 antibody dual-functional mesoporous silica nanoparticles improve tumor immune microenvironment and inhibit YY1-mediated tumor progression. *J Nanobiotechnology*. 2023;21(1):208. doi:10.1186/s12951-023-01967-3

45. Liu S, Sun Y, Jiang M, et al. Glyceraldehyde-3-phosphate dehydrogenase promotes liver tumorigenesis by modulating phosphoglycerate dehydrogenase. *Hepatology*. 2017;66(2):631–645. doi:10.1002/hep.29202

46. Jin H, Shi Y, Lv Y, et al. EGFR activation limits the response of liver cancer to lenvatinib. *Nature*. 2021;595(7869):730–734. doi:10.1038/s41586-021-03741-7

47. Weng YS, Chiang IT, Tsai JJ, Liu YC, Hsu FT. Lenvatinib synergistically promotes radiation therapy in hepatocellular carcinoma by inhibiting Src/STAT3/NF-kappaB-Mediated epithelial-mesenchymal transition and metastasis. *Int J Radiat Oncol Biol Phys*. 2023;115(3):719–732. doi:10.1016/j.ijrobp.2022.09.060

48. Jeon Y, Yoo JE, Rhee H, et al. YAP inactivation in estrogen receptor alpha-positive hepatocellular carcinoma with less aggressive behavior. *Exp Mol Med*. 2021;53(6):1055–1067. doi:10.1038/s12276-021-00639-2

49. Park EJ, Lee JH, Yu GY, et al. Dietary and genetic obesity promote liver inflammation and tumorigenesis by enhancing IL-6 and TNF expression. *Cell*. 2010;140(2):197–208. doi:10.1016/j.cell.2009.12.052

50. Zhang L, Zhang C, Xing Z, et al. Fibronectin 1 derived from tumor-associated macrophages and fibroblasts promotes metastasis through the JUN pathway in hepatocellular carcinoma. *Int Immunopharmacol*. 2022;113(Pt A):109420. doi:10.1016/j.intimp.2022.109420

51. Xu X, Lei Y, Chen L, et al. Phosphorylation of NF-kappaBp65 drives inflammation-mediated hepatocellular carcinogenesis and is a novel therapeutic target. *J Exp Clin Cancer Res*. 2021;40(1):253. doi:10.1186/s13046-021-02062-x

52. Lam YK, Yu J, Huang H, et al. TP53 R249S mutation in hepatic organoids captures the predisposing cancer risk. *Hepatology*. 2023;78(3):727–740. doi:10.1002/hep.32802

53. Makino Y, Hikita H, Kato S, et al. STAT3 is activated by CTGF-mediated tumor-stroma cross talk to promote HCC progression. *Cell Mol Gastroenterol Hepatol*. 2023;15(1):99–119. doi:10.1016/j.jcmgh.2022.09.006

54. Yuan K, Lei Y, Chen HN, et al. HBV-induced ROS accumulation promotes hepatocarcinogenesis through Snail-mediated epigenetic silencing of SOCS3. *Cell Death Differ*. 2016;23(4):616–627. doi:10.1038/cdd.2015.129

55. Zhang H, Song Y, Yang H, et al. Tumor cell-intrinsic Tim-3 promotes liver cancer via NF-κB/IL-6/STAT3 axis. *Oncogene*. 2018;37(18):2456–2468. doi:10.1038/s41388-018-0140-4